China Ocean Eng., 2022, Vol. 36, No. 3, P. 403–412
DOI: https://doi.org/10.1007/s13344-022-0036-5, ISSN 0890-5487
http://www.chinaoceanengin.cn/ E-mail: coe@nhri.cn

Investigation on Effects of Vertical Degree of Freedom on Gap Resonance Between Two Side-by-Side Boxes Under Wave Actions

HE Zhi-wei[a], GAO Jun-liang[a, b, *], SHI Hua-bin[b], ZANG Jun[c], CHEN Hong-zhou[d], LIU Qian[a]

[a] School of Naval Architecture and Ocean Engineering, Jiangsu University of Science and Technology, Zhenjiang 212100, China

[b] State Key Laboratory of Internet of Things for Smart City and Department of Civil and Environmental Engineering, University of Macau, Macao 999078, China

[c] Centre for Infrastructure, Geotechnical and Water Engineering (IGWE), Department of Architecture and Civil Engineering, University of Bath, BA2 7AY, UK

[d] School of Civil Engineering and Architecture, Northeast Electric Power University, Jilin 132012, China

Received August 6, 2021; revised February 15, 2022; accepted March 18, 2022

Abstract

The possible wave resonance in the narrow gap formed by the parallel arrangement of ships will lead to the sharp increase of wave loads and the rapid growth of motion response. The fluid resonance inside a narrow gap between two side-by-side boxes is investigated numerically based on an open-source CFD package, OpenFOAM. The upstream box remains fixed, while the downstream box is allowed to heave freely under wave actions. This work aims to examine the influence of the motion of the downstream box on the fluid resonant behaviors inside the gap. The hydrodynamic behaviors considered include the wave height inside the gap, the heave displacement, and the reflection, transmission, and energy loss coefficients. Gao et al. (2021) reported the influence of the motion of the upstream box on gap resonant behaviors. For comparative study, some results of Gao et al. (2021) are also presented in this work. It is found that the heave motion of any box in the two-box system leads to a smaller resonant wave height amplification and a larger fluid resonance frequency. The frequency at which the maximum heave displacement of the downstream box occurs is less than the fluid resonant frequency. The heave motion of any box in the two-box system results in a larger reflection coefficient and a smaller energy loss coefficient.

Key words: gap resonance, wave height amplification, heave motion, OpenFOAM

Citation: He, Z. W., Gao, J. L., Shi, H. B., Zang, J., Chen, H. Z., Liu, Q., 2022. Investigation on effects of vertical degree of freedom on gap resonance between two side-by-side boxes under wave actions. China Ocean Eng., 36(3): 403–412, doi: https://doi.org/10.1007/s13344-022-0036-5

1 Introduction

For effective exploitation and transportation of marine oil and gas resources, floating liquefied natural gas (FLNG) platforms and liquefied natural gas (LNG) carriers in side-by-side operation are widely used. This kind of side-by-side operation greatly shortens the distance of LNG transportation from the FLNG platform to the LNG carrier. However, one disadvantage of this arrangement is that the large motion of the LNG carrier affects the safety of offloading operations. Under the wave incidence with a specific frequency, the water body trapped in the narrow gap between the FLNG platform and the LNG carrier may resonate. The resonance of the water body will lead to the increase of the wave load acting on the hull, causing the significant motion response of the LNG carrier. This kind of resonant motion of the water body occurring inside the narrow gap is normally called "*gap resonance*" in the literature. Gap resonance has many resonant modes, among which the piston mode is normally the most dangerous for ships because it will lead to large wave loads acting on them.

The gap resonance phenomenon between two or more marine structures has been studied extensively through experimental tests, theoretical analysis, and numerical simulations over the past two decades. Many physical experiments have been performed to investigate the gap resonance. The gap resonance between two stationary bodies has been studied by Saitoh et al. (2006) in a physical wave flume. It was found that the resonant wave height in the gap could reach

Foundation item: This research is financially supported by the National Natural Science Foundation of China (Grant Nos. 51911530205 and 51809039), the Natural Science Foundation of Jiangsu Province (Grant No. BK20201455), the Natural Science Foundation of the Jiangsu Higher Education Institutions (Grant No. 20KJD170005) and the Qing Lan Project of Jiangsu Universities. The work is also partially supported by UK EPSRC (Grant No. EP/T026782/1), the Royal Academy of Engineering (Grant No. UK-CIAPP/73), and the Royal Society (Grant No. IEC\NSFC\181321)..
*Corresponding author. E-mail: gaojunliang880917@163.com

up to five times the incident wave height when the gap resonance occurred. Iwata et al. (2007) further extended their work to the hydrodynamic resonance of three identical bodies with two narrow gaps by laboratory tests. They suggested that the number of gaps or bodies significantly affected the characteristics of gap resonance. Through physical experiments, Ning et al. (2018) investigated the fluid resonance in the gap formed by two barges with different drafts. The results showed that the fluid resonant frequency decreased as the barge draft increased. Tan et al. (2019) experimentally examined the effects of various corner radii on both the wave height amplification and the fluid resonant frequency in the narrow gap between two fixed bodies. Besides, the gap resonance between a fixed box and a bottom-mount vertical wall has also been experimentally studied (e.g., He et al., 2021a; Kristiansen and Faltinsen, 2009; Tan et al., 2014).

Conventional linear potential flow models (Faltinsen et al., 2007; Molin, 2001) and nonlinear ones (Feng and Bai, 2015; Sun et al., 2015) were found to be able to predict the fluid resonant frequencies accurately and capture the resonant modes. However, it is well known that the potential flow theory over-predicts the resonant wave height in the gap when compared with the experimental results because it fails to consider the energy dissipation caused by the fluid viscosity, vortex shedding, and flow separations. Therefore, to consider viscous dissipation, various artificial energy damping methods have been introduced into the potential flow theory (Chen et al., 2011; Chen, 2004; Feng et al., 2018). When the damping coefficient has been successfully calibrated based on available experimental data or CFD (Computational Fluid Dynamics) results, the modified potential flow model can predict the resonance amplitude with reasonable accuracy (Lu et al., 2011a, 2011b; Pauw et al., 2007; Tan et al., 2017).

Based on the incompressible Navier−Stokes equations, the viscous fluid models have also been used to investigate the gap resonance problem (e.g., Feng et al., 2017; He et al., 2021b; Jiang et al., 2019b; Lu et al., 2010, 2020). Based on an open-source CFD package, OpenFOAM, Moradi et al. (2015) investigated the fluid resonance in the gap formed by twin barges with rounded bilges and found that the resonant wave amplitude may reach as high as eleven times the incident wave amplitude. Jiang et al. (2018) studied the wave resonance in the narrow gap between two side-by-side non-identical boxes. Recently, by using OpenFOAM, Gao et al. (2019b, 2020a) examined the gap resonance between two fixed boxes under the regular waves and focused wave groups actions, respectively. Besides the gap resonance between two fixed boxes, Gao et al. (2019a, 2020b) also studied the gap resonance between a fixed box and a vertical wall. Their results suggested that the viscous fluid models can predict both the resonant frequency and resonant amplitude very well.

Most of the studies mentioned above considered the fluid resonance between fixed bodies. However, in most practical engineering problems, marine structures may move under wave actions. For example, an LNG carrier may have the heave motion under wave actions during offloading operations. Sun et al. (2011) investigated the gap resonance between two floating bodies with rigid, hinge, or spring connections. The results showed that the connection condition significantly affected the wave response in the gap and the motion of the bodies. Perić and Swan (2015) experimentally studied the wave resonance in the gap between a floating body and a bottom-mounted wall. They found that the motion of the body led to an increase in the fluid resonant frequency. Li and Teng (2015) studied the wave resonance between two freely rolling barges and reported a jump phenomenon for the wave response in the gap. However, their studies did not consider the effects of the motion of a single body on the gap resonance phenomenon. Li (2019) and Li and Zhang (2016) studied the gap resonance between two forced heave barges. Gao et al. (2021) investigated the gap resonance between a two-box system, in which the upstream box heaved freely and the downstream box remained fixed, and compared it with the gap resonance between another two-box system with both boxes fixed. The current work is a direct extension of Gao et al. (2021). In the present work, we focus on the gap resonance formed inside a two-box system where the downstream box heaves freely and the upstream box remains fixed. For comparison, some results of that paper are also presented in this work.

This paper is organized as follows: the numerical model used in this study and the set-up of the numerical flume will be described in Sections 2 and 3, respectively. The numerical results and discussion are presented in Section 4. Conclusions are finally drawn in Section 5.

2 Description of numerical model

Based on the third-party toolbox waves2Foam in OpenFOAM, the solver waveDyMFoam (Bruinsma et al., 2018) was applied to solve the Navier−Stokes equations for water and air. The governing equations are the Navier−Stokes equations in the Arbitrary Lagrangian−Eulerian (ALE) reference frame,

$$\frac{\partial \rho u_i}{\partial x_i} = 0; \tag{1}$$

$$\frac{\partial \rho u_i}{\partial t} + \frac{\partial \rho \left(u_j - u_j^m\right) u_i}{\partial x_j} = \rho f_i - \frac{\partial p}{\partial x_i} + \mu \frac{\partial}{\partial x_j}\left(\frac{\partial u_i}{\partial x_j} + \frac{\partial u_j}{\partial x_i}\right), \tag{2}$$

where u_i is the fluid velocity component in the i-th (i = 1, 2, 3) direction, p is the dynamic pressure, ρ is the fluid density, f_i is the external body force, μ is the fluid dynamic viscosity, and u_i^m is the velocity component of the deformed computational meshes accounting for the fluid and structure interaction.

The volume of fluid (VOF) method (Hirt and Nichols, 1981) is used to capture the motion of the free surface. In a computational cell, the fractional function of VOF, γ, is defined as follows:

$$\gamma = \begin{cases} 0, & \text{in air} \\ 0 < \gamma < 1, & \text{on the surface} \\ 1, & \text{in water} \end{cases} \tag{3}$$

The contour of the VOF function $\gamma = 0.5$ is used to represent the interface between the water and air phases. The distribution of γ is calculated by the following advection equation:

$$\frac{\partial \gamma}{\partial t} + \left(u_i - u_i^m\right)\frac{\partial \gamma}{\partial x_i} + \nabla \cdot [\boldsymbol{u}_\mathrm{r}\gamma(1-\gamma)] = 0, \tag{4}$$

where $\boldsymbol{u}_\mathrm{r}$ is the relative velocity between two phases. In the simulations, the effective fluid density and the viscosity can be expressed as follows:

$$\rho = \gamma\rho_{\mathrm{water}} + (1-\gamma)\rho_{\mathrm{air}}, \tag{5}$$

$$\mu = \gamma\mu_{\mathrm{water}} + (1-\gamma)\mu_{\mathrm{air}}, \tag{6}$$

respectively, where subscripts "water" and "air" represent the water and air phases, respectively.

The generation and the elimination of waves in the waves2Foam library are simulated by setting parameters of relaxation zone. The numerical simulations start from the static state, which means that the initial conditions are zero dynamic pressure and zero fluid velocity. For the inlet boundary, the velocity is set as the incident wave velocity, and the pressure gradient is zero. The boundary condition of the solid walls is no-slip. The boundary condition of the upper boundary of the computation domain is "atmosphere".

The governing equations are solved by the finite volume method (FVM). The velocity and pressure are solved by the PISO (pressure implicit with the splitting of the operator) algorithm (Jasak, 1996). The convection term is discretized by the Gauss limited linear method, and the diffusion term is discretized by the Gauss linear corrected method. For details of the numerical schemes, readers can see Jasak (1996). With the 6-DOF rigid-body motion solver built in OpenFOAM, the motions of the floating body are calculated. The time step Δt is automatically adjusted by the Courant-Friedrichs-Lewy (CFL) condition, and the largest allowed Courant Number is set to $C_\mathrm{r} = 0.25$.

3 Numerical wave flume

Fig. 1 shows the two-dimensional (2D) numerical wave flume adopted in this study. The size of the flume is 18.5 m in length and 0.9 m in height. The coordinate system is defined as follows. The origin is located at the static water level (SWL), the wave propagation direction is the x-axis, and the upward direction is the y-axis. Two identical rectangular boxes are placed in the middle of the wave flume with a water depth h is 0.5 m. The breadth B of the two boxes is 0.5 m, and the draft d is 0.25 m. The two boxes form a narrow gap with the breadth $B_\mathrm{g} = 0.05$ m.

Five incident wave heights are considered in this study, i.e., H_0 = 0.01, 0.02, 0.03, 0.04, and 0.05 m. The regular waves are generated at the inlet boundary by using the second-order Stokes theory. The wave frequency considered in this work ranges from 4.947 rad/s to 6.323 rad/s (equivalently, the dimensionless wavenumber kh varies from 2.10 to 1.41). As shown in Fig. 1, five wave gauges, G_1–G_5, are equipped to record the wave elevation. G_1 and G_2 with a distance of 0.25 m are used to separate the incident and the reflected waves. To record the free-surface elevations in front of the upstream box and inside the gap, G_3 and G_4 are situated at 0.005 m from the left side of the upstream box and in the middle of the gap, respectively. G_5 is used to record the transmission waves, which is located 1.5 m to the right of downstream box. Two relaxation zones with a length of 6.0 m are arranged on the left and right sides of the wave flume, respectively.

Fig. 2 shows a typical mesh in the vicinity of two boxes. The non-uniform meshes are adopted to save the simulation time. The finer meshes with higher resolution are adopted around two boxes, especially in the vicinity of the gap. The mesh dependency tests are carried out by using three different meshes, i.e., Mesh 1, Mesh 2, and Mesh 3. Table 1 lists the details of the three meshes. Based on the results shown in

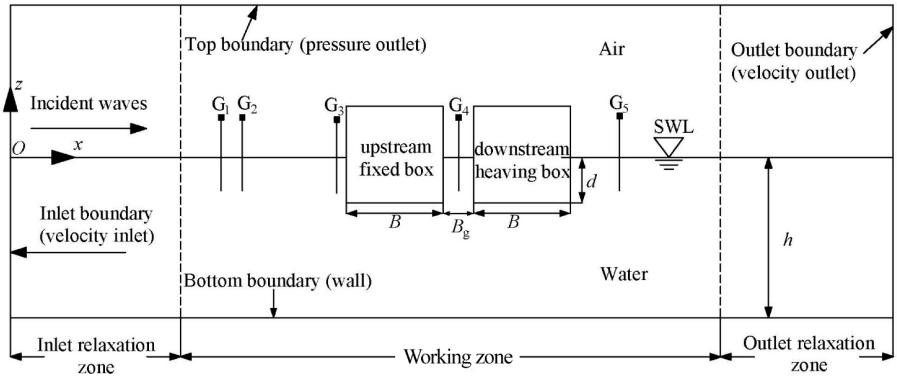

Fig. 1. Sketch of the numerical wave flume.

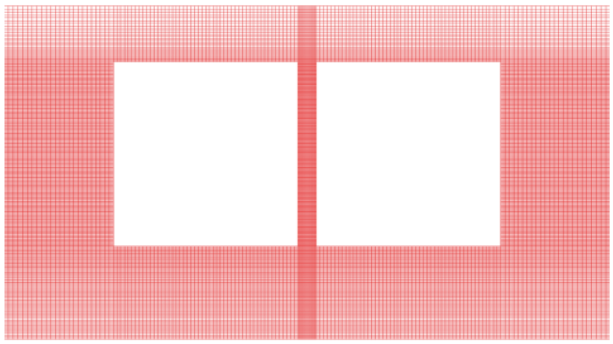

Fig. 2. Typical computational meshes in the vicinity of two boxes.

Table 1 Details of Mesh 1, Mesh 2, and Mesh 3

Mesh	No. of cells	No. of points	No. of faces	Size of cells across the gap (m)	
				Δx	Δz
Mesh 1	79850	161548	320325	0.0050	0.0040
Mesh 2	211960	426970	849366	0.0031	0.0020
Mesh 3	317400	638338	1271370	0.0025	0.0016

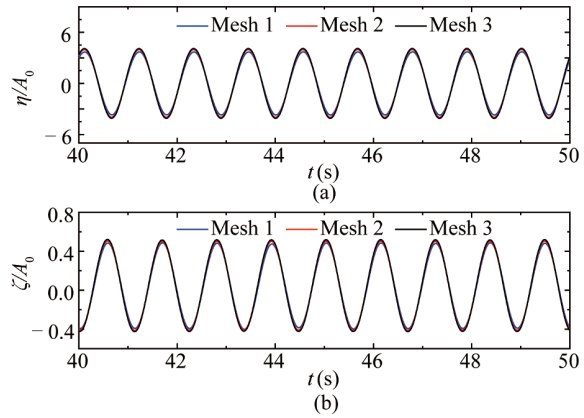

Fig. 3. Mesh dependence tests for (a) the free surface elevation in the gap and (b) the heave displacement of downstream box under wave actions with kh = 1.73 and H_0 = 0.01 m.

Section 4.1, for the down-heave structure system subjected to the incident waves with H_0 = 0.01 m, the fluid resonant frequency is kh = 1.73. Fig. 3 shows the time histories of the free surface elevation in the gap and the heave displacement of the downstream box excited by the incident waves with H_0 = 0.01 m and kh = 1.73. The comparison shown in Fig. 3 indicates that the convergent results have been obtained by Mesh 2. Hence, Mesh 2 is selected in all the simulations of the present work. The total simulation time is 50.0 s. It can be seen from Fig. 3 that both the free-surface elevation in the gap and the heave motion of the downstream box have reached a steady-state after t = 30.0 s. The numerical results in the following section are based on their steady-state time histories from 30.0 to 50.0 s.

In Gao et al. (2021), a few preliminary verifications on the accuracy of the numerical model have already been conducted for the wave height amplification inside the gap formed by two fixed boxes and for the heave motion of one box under wave actions. More verifications of the model for the gap resonance phenomenon can also be seen in Moradi et al. (2016), Jiang et al. (2019a), Jiang et al. (2018), Tan et al. (2021) and Lu et al. (2020).

4 Results and discussion

To understand the effect of the heave motion of downstream box on gap resonance between two boxes, several hydrodynamic characteristics of gap resonance are discussed in this section, including the wave height amplification in the gap, the heave displacement of the downstream box, reflection coefficient, transmission coefficient, and energy dissipation coefficient. Gao et al. (2021) studied the gap resonance between two fixed boxes and between an upstream heaving box and a downstream fixed box. For comparative study, some results of these two structure systems are also presented in this work. To simplify the description, the two-box system in which the upstream box heaves freely and the downstream box keeps fixed is called “up-heave structure system”; the two-box system in which the downstream box heaves freely and the upstream box keeps fixed is called “down-heave structure system”; the two-box system with both boxes fixed is referred to as “fixed structure system”.

4.1 Wave height amplification

Fig. 4 shows the time histories of the free-surface elevation inside the gap for the down-heave structure system excited by the incident waves with H_0 = 0.01 m at the fluid resonant frequency. For the down-heave structure system, the fluid resonant frequency is kh = 1.730. It can be observed from Fig. 4 that the resonant wave height amplification for the down-heave structure system is 3.975, while based on Gao et al. (2021), for the fixed and the up-heave structure systems, the resonant wave height amplifications are 6.596 and 4.64, respectively (the red and blue lines in Fig. 4 present the resonant free-surface elevations for the fixed and the up-heave structure systems, respectively). It is implied that the resonant wave height amplification for the down-heave structure system is smaller than that for the fixed structure system.

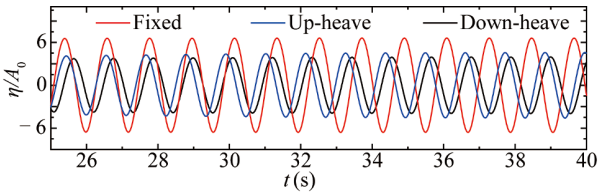

Fig. 4. Time histories of the free-surface elevation inside the gap for the three structure systems excited by incident waves with H_0 = 0.01 m at their respective fluid resonant frequency. For the down-heave structure system, the fluid resonant frequency is kh = 1.730.

Fig. 5 shows the wave height amplifications inside the gap under the conditions of various incident wave heights. For comparison, this figure also presents the wave height

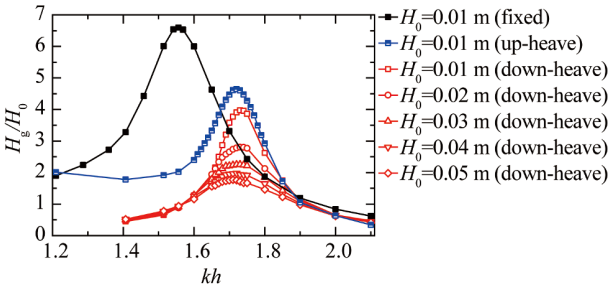

Fig. 5. Overall wave height amplification inside the gap excited by the incident waves with various wave heights.

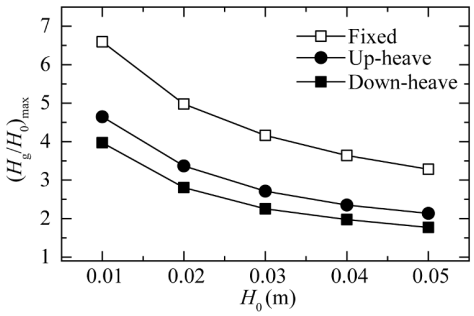

Fig. 7. Comparison of the resonant wave height amplification, $(H_g/H_0)_{max}$, for various incident wave heights.

amplifications inside the gap for the fixed and the up-heave structure systems for H_0 = 0.01 m. The following four phenomena can be observed. Firstly, similar to both the fixed and the up-heave structure systems, the variation trend of the wave height amplification with the incident wave frequency shows a single peak shape. That is, the maximum wave height amplification occurs at a single fluid resonant frequency for each incident wave height. Secondly, the fluid resonant frequency of the down-heave structure system seems to decrease gradually with the incident wave height. To better show this decreasing trend, Fig. 6 further illustrates the variation of the fluid resonant frequency with the incident wave height. The fluid resonant frequencies for both the fixed and the up-heave structure systems are also shown in this figure. The second phenomenon can be observed more intuitively from Fig. 6. Besides, the fluid resonant frequencies for both the up-heave and the down-heave structure systems are always larger than those for the fixed structure system, and the fluid resonant frequencies for the down-heave structure system are always larger than those for the up-heave structure system.

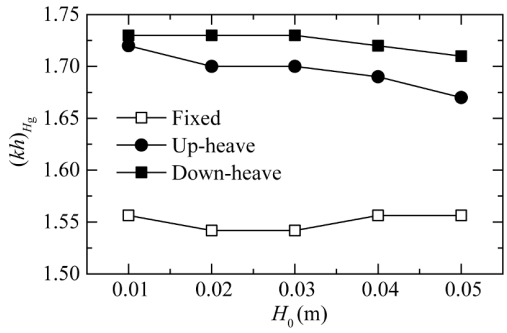

Fig. 6. Variation of the fluid resonant frequency, $(kh)_{Hg}$, with the incident wave height.

Thirdly, the resonant wave height amplification inside the gap decreases with the increase of the incident wave height. Fig. 7 further shows the resonant wave height amplification, $(H_g/H_0)_{max}$, at various incident wave heights. The resonant wave height amplifications for the fixed and the up-heave structure systems are also shown in this figure for comparison. It is seen that the resonant wave height amplifications for all the three structure systems monotonically decrease with the increase of the incident wave height and that the down-heave structure system always has the lowest wave height amplification among the three structure systems. This can be attributed to the fact that the reflection coefficient at fluid resonant frequency increases with the increase of incident wave height (see Section 4.3), resulting in the decrease of wave energy entering the gap. Hence, the resonant wave height amplification inside the gap decreases. Moreover, for the down-heave structure system, part of the wave energy transmitted into the gap is converted into the mechanical energy of downstream box, which further reduces the resonant wave height inside the gap, and makes the resonant wave height inside the gap smaller than that for the up-heave structure system whose mechanical energy of upstream box directly comes from the incident wave energy.

Fourthly, Fig. 8 shows the velocity vectors and the vorticity contours over one period for the case with H_0 = 0.01 m at the fluid resonant frequency kh = 1.730 for the down-heave structure system. Fig. 8a corresponds to the instant that the free water surface in the gap is near the still water level (i.e., $\eta \approx 0$). At this moment (t = 0), the shear layers along the bottoms of the two boxes and the vertical sidewalls of the gap can be seen, where a pair of vortices a^+ and a^- are being generated. The other pair of vortices b^+ and b^- are located below the two boxes. At $t = T/4$ (Fig. 8b), the free water surface in the gap reaches the highest position, implying the fluid begins to flow out of the gap. The vortices a^+ and a^- develop and fall off the corner of the two boxes. When $t = 2T/4$ (Fig. 8c), the vortices a^+ and a^- flow out of the gap as the fluid flows. At this instant, a new pair of vortices c^+ and c^- develop from the edge profiles of the two boxes. As the time elapses, the free surface in the gap reaches the lowest position at $t = 3T/4$ (Fig. 8d). The vortices a^+ and a^- and c^+ and c^- flow out of the gap as the fluid flows. The vortices c^+ and c^- finally form beneath the corner of the two boxes.

4.2 Heave displacement of the downstream box

Fig. 9 presents the heave displacement of the downstream box excited by the incident wave with various wave heights. This figure also shows the heave displacements of the

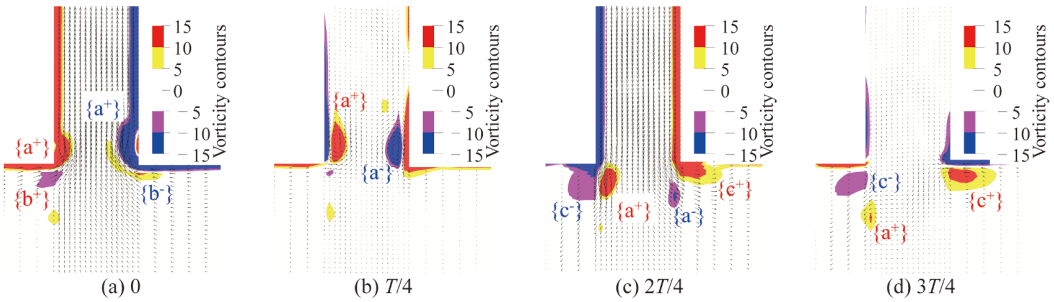

Fig. 8. Velocity vectors and vorticity contours during one period of the incident waves with $T/4$ interval at the fluid resonant frequency kh = 1.730 for the down-heave structure system with H_0 = 0.01 m

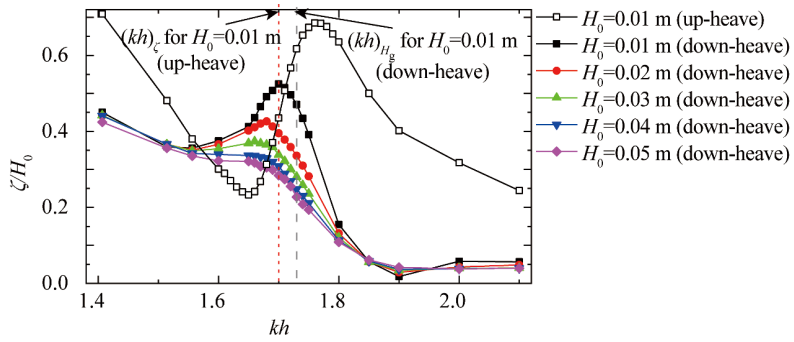

Fig. 9. Heave displacement of the downstream box excited by the incident wave with various wave heights. $(kh)_\zeta$ represents the incident wave frequency at which the maximum heave displacement of the downstream box occurs.

upstream box for the up-heave structure system. The heave displacement ζ is normalized by the incident wave height H_0. $(kh)_\zeta$ in the figure represents the incident wave frequency at which the maximum heave displacement of the downstream box occurs. The following three phenomena can be seen from the figure. Firstly, the heave displacement of the downstream box for the down-heave structure system always first decreases, then increases, and then decreases with the increase of the incident wave frequency. This variation trend is similar to the heave displacement for the up-heave structure system, but the values of their turning points are different. In addition, the value of heave displacement in the high-frequency range (kh>1.9) is much smaller than that in other frequency ranges. It may be attributed to the fact that the reflection coefficient is much larger in the high-frequency range (see Section 4.3), the wave energy transmitted into the narrow gap becomes much lower, and finally the energy converted into the mechanical energy of the downstream box is significantly reduced.

Secondly, the wave frequency $(kh)_\zeta$ at which the maximum heave displacement of the downstream box occurs appears to be different for various incident wave heights. To show this phenomenon more clearly, Fig. 10 illustrates the wave frequency at which the maximum heave displacement of the downstream box occurs $(kh)_\zeta$ for all the incident wave heights. For comparison, the wave frequencies $(kh)_\zeta$ at which the maximum heave displacement of the upstream box occurs for the up-heave structure system are also shown in this figure. The frequency $(kh)_\zeta$ for the down-heave structure system decreases with the increase of the incident wave height while that for the up-heave structure system slightly fluctuates around kh=1.760. Besides, by carefully comparing Fig. 6 with Fig. 10, it can be found that for the down-heave structure system, the frequency $(kh)_\zeta$ is always less than the fluid resonant frequency, regardless of the incident wave height. However, for the up-heave structure system, the former is always larger than the latter.

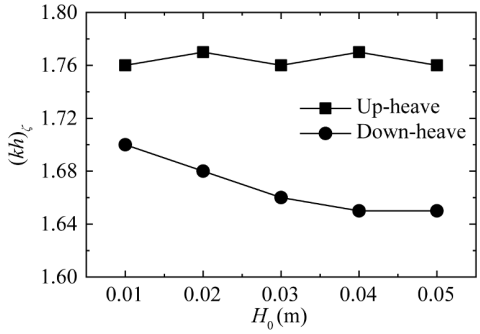

Fig. 10. Wave frequency at which the maximum heave displacement occurring for different incident wave heights.

Thirdly, as the incident wave height increases, the maximum value of the normalized heave displacement presents a decreasing trend. Fig. 11 further shows the maximum normalized heave displacement for various incident wave heights. The maximum normalized heave displacements for

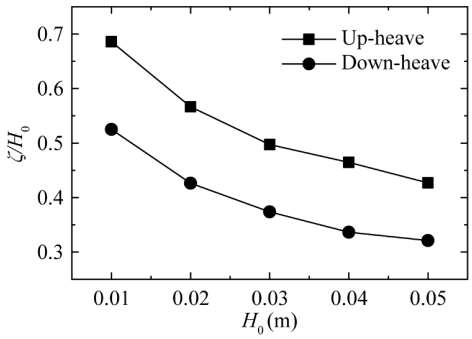

Fig. 11. Comparison of the maximum normalized heave displacement for various incident wave heights

both structure systems decrease gradually with the increase of the incident wave height, and the heave displacement for the down-heave structure system is always notably smaller than that for the up-heave structure system. Furthermore, taking the side-by-side loading operation of LNG ship and FLNG platform as the background, under certain incident wave height, the maximum displacement of floating body reflects its potential most unfavorable condition. Therefore, readers can quickly evaluate the variation of the potential most unfavorable condition with the incident wave height and incoming wave directions.

4.3 Reflection, transmission, and energy loss coefficients

Fig. 12 shows the comparisons of the reflection coefficient for various incident wave heights. The reflected and transmitted waves considered in this section include the radiated waves excited by the heave motion of the downstream box, and it is theoretically impossible and unnecessary for radiated waves to be separated from the reflected and transmitted waves. For the fixed structure system, the reflection coefficient always first decreases and then increases with the wave frequency. However, for the down-heave structure system, the reflection coefficient is shown first to decrease, then increase, and then decrease as the wave frequency increases. Moreover, the minimum value of the reflection coefficient always occurs at or very close to the fluid resonant frequency for both the fixed and the down-heave structure systems. The minimum reflection coefficient gradually increases with the incident wave height, but the degree of the increase of minimum reflection coefficient for the down-heave structure system is not as obvious as that for the fixed structure system.

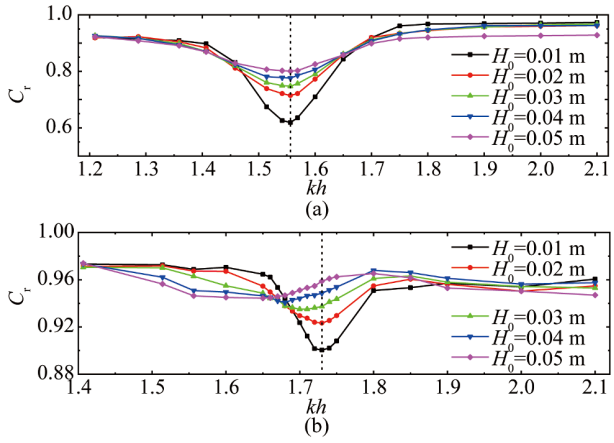

Fig. 12. Comparison of reflection coefficient, C_r, for various incident wave heights: (a) the fixed structure system, (b) the down-heave structure system. The black and red dashed lines representing the fluid resonant frequency for the corresponding structure system when H_0= 0.01 m.

To show the last phenomenon mentioned above more clearly, Fig. 13 shows the variation of the minimum reflection coefficient with respect to the incident wave height for all the three structure systems. The minimum reflection coefficient for each structure system increases with the incident wave height. For both up-heave and down-heave structure systems, the minimum reflection coefficient is remarkably larger than that for the fixed structure system because the radiated waves generated by the heave motion contribute to the reflection waves, resulting in a larger reflection coefficient. In addition, the minimum reflection coefficients for the down-heave structure system are larger than those for the up-heave structure system at various incident wave heights.

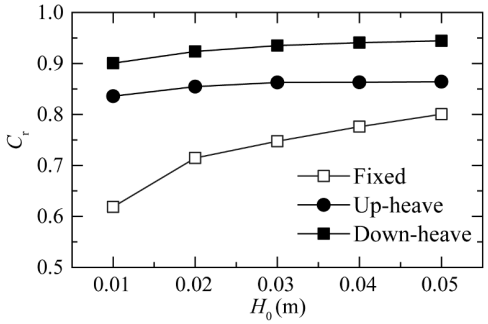

Fig. 13. Comparison of the minimum reflection coefficients for various incident wave heights.

Fig. 14 shows the transmission coefficients, C_t, for various incident wave heights. The variation of transmission coefficient with the wave frequency for the down-heave structure system is different from that for the fixed structure system. For the fixed structure system, the transmission coefficient first increases and then decreases with the incident wave frequency when the incident wave height H_0<0.03 m. With the increase of the incident wave height, the variation trend becomes monotonically decreasing. While for the down-heave structure system, it first decreases, then slightly increases, and then decreases when the incident wave height H_0<0.03 m. For the larger incident wave heights, its variation trend becomes similar to that of the fixed structure system. By comparing Fig. 12 with Fig. 14, it can be found that the reflection coefficient is always larger than the transmission coefficient for all the incident wave heights. In addition, the larger the incident wave height is, the more obvious the dif-

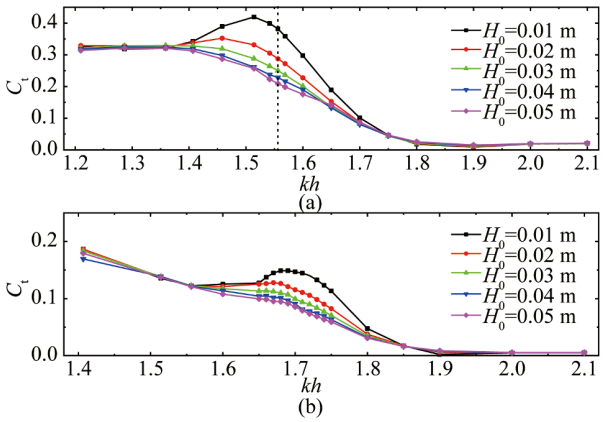

Fig. 14. As in Fig. 12 but for the transmission coefficient, C_t.

ference between the reflection and the transmission coefficients becomes.

The energy loss coefficient, L_e, is defined as $L_e = 1 - C_r^2 - C_t^2$. Fig. 15 shows the energy loss coefficient (L_e) for all the incident wave heights. Different from the fixed structure system, the energy dissipation coefficient for the down-heave structure system first increases, then decreases, and then increases slightly. Its maximum value always appears near the fluid resonance frequency for both structure systems. In addition, the maximum energy loss coefficient decreases gradually with the increase of the incident wave height. To see this tendency more clearly, Fig. 16 shows the variation of the maximum energy loss coefficient with the incident wave heights for all the three structure systems. For both the up-heave and the down-heave structure systems, the maximum energy loss coefficient is less than that for the fixed structure system. This indicates that the heave motion of any box will lead to less energy dissipation during gap resonance. In addition, the maximum energy loss coefficients for the down-heave structure system are always lower than those for the up-heave structure system, no matter whether H_0 is large or small.

5 Conclusions

In this paper, a 2D numerical wave flume based on the

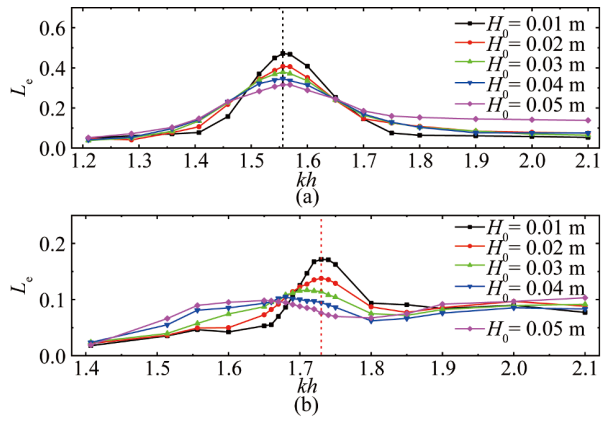

Fig. 15. As in Fig. 12 but for the energy loss coefficient, L_e.

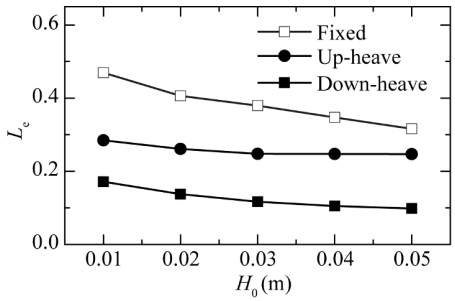

Fig. 16. Comparison of the maximum energy loss coefficients for various incident wave heights.

Navier–Stokes equations is used to investigate the hydrodynamic behaviors of gap resonance formed by two identical boxes. The upstream box keeps fixed, and the downstream box is allowed to heave freely. The influences of the heave motion of the downstream box on the hydrodynamic characteristics of gap resonance are systematically investigated here. Gao et al. (2021) studied the gap resonance between two fixed boxes and between an upstream heaving box and a downstream fixed box. For comparative study, some data from that paper are also presented in this work. To simplify the description, the two-box system in which the upstream box heaves freely and the downstream box keeps fixed is called "up-heave structure system"; the two-box system in which the downstream box heaves freely and the upstream box remains fixed is called "down-heave structure system"; the two-box system with both boxes fixed is referred to as "fixed structure system". The hydrodynamic behaviors considered include the wave height amplification in the gap, the heave displacement of the downstream box, and the reflection, the transmission, and the energy loss coefficients of the two-box system. The main conclusions are drawn as follows.

(1) For both the up-heave and the down-heave structure systems, the resonant wave height amplifications in the gap are always lower than those for the fixed structure system, and the fluid resonant frequencies are always larger than those for the fixed structure system. This indicates that the heave motion of any box in the two-box system will lead to a smaller resonant wave height amplification and a larger fluid resonant frequency. In addition, for the down-heave structure system, the resonant wave height amplification and the fluid resonant frequency are respectively smaller and larger than the corresponding ones for the up-heave structure system.

(2) For the down-heave structure system, the frequency at which the maximum heave displacement occurs is always lower than the corresponding fluid resonant frequency. This is different from the related phenomenon for the up-heave structure system in which the former is shown to be always larger than the latter. The maximum normalized heave displacements for both the up-heave and the down-heave struc-

ture systems decrease gradually with the increase of incident wave height, and the maximum heave displacement for the down-heave structure system is always notably smaller than that for the up-heave structure system.

(3) Both the minimum reflection coefficient and the maximum energy loss coefficient occur at (or very close to) the fluid resonant frequency for all the three structure systems. For both the up-heave and the down-heave structure systems, the minimum reflection coefficients are larger than the corresponding ones for the fixed structure system, and the maximum energy loss coefficients are smaller than the corresponding ones for the fixed structure system. This suggests that the heave motion of any box in the two-box system will lead to a larger wave reflection and a smaller energy loss.

References

Bruinsma, N., Paulsen, B.T. and Jacobsen, N.G., 2018. Validation and application of a fully nonlinear numerical wave tank for simulating floating offshore wind turbines, *Ocean Engineering*, 147, 647–658.

Chen, X.B., 2004. Hydrodynamics in offshore and naval applications-part 1. Keynote lecture, *The 6th International Conference on Hydrodynamics*, Perth, Australia.

Chen, X.B., Duan, W.Y. and Liu, H.X., 2011. Dissipation effect in potential flows of fairly perfect fluid, *Proceedings of 26th International Workshop on Water Waves and Floating Bodies*, Greece, 17–20.

Faltinsen, O.M., Rognebakke, O.F. and Timokha, A.N., 2007. Two-dimensional resonant piston-like sloshing in a moonpool, *Journal of Fluid Mechanics*, 575, 359–397.

Feng, X. and Bai, W., 2015. Wave resonances in a narrow gap between two barges using fully nonlinear numerical simulation, *Applied Ocean Research*, 50, 119–129.

Feng, X., Bai, W., Chen, X.B., Qian, L. and Ma, Z.H., 2017. Numerical investigation of viscous effects on the gap resonance between side-by-side barges, *Ocean Engineering*, 145, 44–58.

Feng, X., Chen, X.B. and Dias, F., 2018. A potential flow model with viscous dissipation based on a modified boundary element method, *Engineering Analysis with Boundary Elements*, 97, 1–15.

Gao, J.L., Chen, H.Z., Zang, J., Chen, L.F., Wang, G. and Zhu, Y.Z., 2020a. Numerical investigations of gap resonance excited by focused transient wave groups, *Ocean Engineering*, 212, 107628.

Gao, J.L., He, Z.W., Huang, X.H., Liu, Q., Zang, J. and Wang, G., 2021. Effects of free heave motion on wave resonance inside a narrow gap between two boxes under wave actions, *Ocean Engineering*, 224, 108753.

Gao, J.L., He, Z.W., Zang, J., Chen, Q., Ding, H.Y. and Wang, G., 2019a. Topographic effects on wave resonance in the narrow gap between fixed box and vertical wall, *Ocean Engineering*, 180, 97–107.

Gao, J.L., He, Z.W., Zang, J., Chen, Q., Ding, H.Y. and Wang, G., 2020b. Numerical investigations of wave loads on fixed box in front of vertical wall with a narrow gap under wave actions, *Ocean Engineering*, 206, 107323.

Gao, J.L., Zang, J., Chen, L.F., Chen, Q., Ding, H.Y. and Liu, Y.Y., 2019b. On hydrodynamic characteristics of gap resonance between two fixed bodies in close proximity, *Ocean Engineering*, 173, 28–44.

He, Z.W., Gao, J.L., Chen, H.Z., Zang, J., Liu, Q. and Wang, G., 2021a. Harmonic analyses of hydrodynamic characteristics for gap resonance between fixed box and vertical wall, *China Ocean Engineering*, 35(5), 712–723.

He, Z.W., Gao, J.L., Zang, J., Chen, H.Z., Liu, Q. and Wang, G., 2021b. Effects of free heave motion on wave forces on two side-by-side boxes in close proximity under wave actions, *China Ocean Engineering*, 35(4), 490–503.

Hirt, C.W. and Nichols, B.D., 1981. Volume of fluid (VOF) method for the dynamics of free boundaries, *Journal of Computational Physics*, 39(1), 201–225.

Iwata, H., Saitoh, T. and Miao, G.P., 2007. Fluid resonance in narrow gaps of very large floating structure composed of rectangular modules, *Proceedings of the 4th International Conference on Asian and Pacific Coasts*, Nanjing, China, pp. 815–826.

Jasak, H., 1996. *Error Analysis and Estimation for the Finite Volume Method with Applications to Fluid Flows*, Ph.D. Thesis, Imperial College, London.

Jiang, S.C., Bai, W., Cong, P.W. and Yan, B., 2019a. Numerical investigation of wave forces on two side-by-side non-identical boxes in close proximity under wave actions, *Marine Structures*, 63, 16–44.

Jiang, S.C., Bai, W. and Tang, G.Q., 2018. Numerical simulation of wave resonance in the narrow gap between two non-identical boxes, *Ocean Engineering*, 156, 38–60.

Jiang, S.C., Sun, Z., Feng, A.H. and Zhang, G.Y., 2019b. On hydrodynamic behavior of fluid resonance in moonpool and its suppression by using various convex appendages, *Ocean Engineering*, 192, 106552.

Kristiansen, T. and Faltinsen, O.M., 2009. Studies on resonant water motion between a ship and a fixed terminal in shallow water, *Journal of Offshore Mechanics and Arctic Engineering*, 131(2), 021102.

Li, S. and Teng, B., 2015. Numerical examination of wave-induced coupling roll motion and fluid resonance between twin floating barges in proximity, *Procedia Engineering*, 126, 242–246.

Li, Y.J., 2019. Fully nonlinear analysis of second-order gap resonance between two floating barges, *Engineering Analysis with Boundary Elements*, 106, 1–19.

Li, Y.J. and Zhang, C.W., 2016. Analysis of wave resonance in gap between two heaving barges, *Ocean Engineering*, 117, 210–220.

Lu, L., Cheng, L., Teng, B. and Sun, L., 2010. Numerical simulation and comparison of potential flow and viscous fluid models in near trapping of narrow gaps, *Journal of Hydrodynamics*, 22(1), 120–125.

Lu, L., Tan, L., Zhou, Z.B., Zhao, M. and Ikoma, T., 2020. Two-dimensional numerical study of gap resonance coupling with motions of floating body moored close to a bottom-mounted wall, *Physics of Fluids*, 32(9), 092101.

Lu, L., Teng, B., Cheng, L., Sun, L. and Chen, X.B., 2011a. Modelling of multi-bodies in close proximity under water waves—Fluid resonance in narrow gaps, *Science China Physics, Mechanics and Astronomy*, 54(1), 16–25.

Lu, L., Teng, B., Sun, L. and Chen, B., 2011b. Modelling of multi-bodies in close proximity under water waves—Fluid forces on floating bodies, *Ocean Engineering*, 38(13), 1403–1416.

Molin, B., 2001. On the piston and sloshing modes in moonpools, *Journal of Fluid Mechanics*, 430, 27–50.

Moradi, N., Zhou, T.M. and Cheng, L., 2015. Effect of inlet configuration on wave resonance in the narrow gap of two fixed bodies in close proximity, *Ocean Engineering*, 103, 88–102.

Moradi, N., Zhou, T.M. and Cheng, L., 2016. Two-dimensional numerical study on the effect of water depth on resonance behaviour of the fluid trapped between two side-by-side bodies, *Applied Ocean*

Research, 58, 218–231.

Ning, D.Z., Zhu, Y., Zhang, C.W. and Zhao, M., 2018. Experimental and numerical study on wave response at the gap between two barges of different draughts, *Applied Ocean Research*, 77, 14–25.

Pauw, W.H., Huijsmans, R.H.M. and Voogt, A., 2007. Advances in the hydrodynamics of side-by-side moored vessels, *Proceedings of the ASME 2007 26th International Conference on Offshore Mechanics and Arctic Engineering*, ASME, San Diego, California, USA.

Perić, M. and Swan, C., 2015. An experimental study of the wave excitation in the gap between two closely spaced bodies, with implications for LNG offloading, *Applied Ocean Research*, 51, 320–330.

Saitoh, T., Miao, G.P. and Ishida, H., 2006. Theoretical analysis on appearance condition of fluid resonance in a narrow gap between two modules of very large floating structure, *Proceedings of the 3rd Asia-Pacific Workshop on Marine Hydrodynamics*, Shanghai, pp. 170–175.

Sun, L., Taylor, R.E. and Choo, Y.S., 2011. Responses of interconnected floating bodies, *The IES Journal Part A*: *Civil & Structural Engineering*, 4(3), 143–156.

Sun, L., Taylor, R.E. and Taylor, P.H., 2015. Wave driven free surface motion in the gap between a tanker and an FLNG barge, *Applied Ocean Research*, 51, 331–349.

Tan, L., Cheng, L. and Ikoma, T., 2021. Damping of piston mode resonance between two fixed boxes, *Physics of Fluids*, 33(6), 062117.

Tan, L., Lu, L., Liu, Y., Sabodash, O.A. and Teng, B., 2014. Dissipative effects of resonant waves in confined space formed by floating box in front of vertical wall, *Proceedings of the Eleventh* (*2014*) *Pacific/Asia Offshore Mechanics Symposium*, The International Society of Offshore and Polar Engineers, Shanghai, China.

Tan, L., Lu, L., Tang, G.Q., Cheng, L. and Chen, X.B., 2019. A viscous damping model for piston mode resonance, *Journal of Fluid Mechanics*, 871, 510–533.

Tan, L., Tang, G.Q., Zhou, Z.B., Cheng, L., Chen, X.B. and Lu, L., 2017. Theoretical and numerical investigations of wave resonance between two floating bodies in close proximity, *Journal of Hydrodynamics*, 29(5), 805–816.